Cite this: *Phys. Chem. Chem. Phys.*, 2011, **13**, 18115–18122

www.rsc.org/pccp

PAPER

Investigation of CO_2 capture mechanisms of liquid-like nanoparticle organic hybrid materials *via* structural characterization†

Youngjune Park,[a] John Decatur,[b] Kun-Yi Andrew Lin[a] and Ah-Hyung Alissa Park*[a]

Received 16th August 2011, Accepted 26th August 2011
DOI: 10.1039/c1cp22631b

Nanoparticle organic hybrid materials (NOHMs) have been recently developed that comprise an oligomeric or polymeric canopy tethered to surface-modified nanoparticles *via* ionic or covalent bonds. It has already been shown that the tunable nature of the grafted polymeric canopy allows for enhanced CO_2 capture capacity and selectivity *via* the enthalpic intermolecular interactions between CO_2 and the task-specific functional groups, such as amines. Interestingly, for the same amount of CO_2 loading NOHMs have also exhibited significantly different swelling behavior compared to that of the corresponding polymers, indicating a potential structural effect during CO_2 capture. If the frustrated canopy species favor spontaneous ordering due to steric and/or entropic effects, the inorganic cores of NOHMs could be organized into unusual structural arrangements. Likewise, the introduction of small gaseous molecules such as CO_2 could reduce the free energy of the frustrated canopy. This entropic effect, the result of unique structural nature, could allow NOHMs to capture CO_2 more effectively. In order to isolate the entropic effect, NOHMs were synthesized without the task-specific functional groups. The relationship between their structural conformation and the underlying mechanisms for the CO_2 absorption behavior were investigated by employing NMR and ATR FT-IR spectroscopies. The results provide fundamental information needed for evaluating and developing novel liquid-like CO_2 capture materials and give useful insights for designing and synthesizing NOHMs for more effective CO_2 capture.

Introduction

In the past few decades, organic–inorganic hybrid materials have received great attention in a number of scientific and engineering fields because of their versatile properties. In particular, polymer grafted nanoparticles have been the main research topic for the fields focusing on the novel platform for polymer synthesis,[1,2] dispersion and blending of nanostructures,[3,4] and self-assembly of hybrid materials.[5,6]

Recently developed nanoparticle organic hybrid materials (NOHMs) are an emerging class of self-suspended nanoparticle systems.[7,8] They are created by ionically or covalently grafting organic oligomers or polymers onto surface-modified inorganic nanoparticles. Because each particle shares its suspending liquid of grafted organic species, this allows NOHMs to exhibit self-suspended, liquid-like behavior with unusual dynamic features.[9,10] Until now, a series of different types of NOHMs have been synthesized using metal oxides,[7–14] metals,[15–18] carbon nanotubes,[19,20] and proteins[21] as cores. For each rheologically different NOHMs, ranging from glassy solids to solvent-free nanoparticle suspensions, various physicochemical properties, such as thermodynamical, electrical, and optical properties, can be tuned by altering their inorganic nanoparticles and organic canopies.

NOHMs show enhanced thermal stability with negligible vapor pressure compared to pure oligomers or polymers; thus, NOHMs can be used as a 'green' solvent. Consequently, NOHMs can be employed in a variety of applications as novel thermal management materials, reaction solvents, magnetic fluids, conductive lubricants, nanocomposite materials, electrolytes *etc.*[10,22] Another interesting property of NOHMs is their solvating ability, which allow them to be applied to various separation and capture processes.

With an increasing interest and debate over global climate changes, capturing and removing anthropogenic CO_2 has become a global and urgent issue. Several methods have been proposed to capture CO_2 from large point sources, especially

[a] *Department of Earth and Environmental Engineering & Department of Chemical Engineering, and Lenfest Center for Sustainable Energy, Columbia University, New York, NY 10027, USA. E-mail: ap2622@columbia.edu; Fax: +1 212 854 7081; Tel: +1 212 854 8989*
[b] *Department of Chemistry, Columbia University, New York, NY 10027, USA*

† Electronic supplementary information (ESI) available: 2D NMR results; AFM and TEM images; ATR FT-IR results. See DOI: 10.1039/c1cp22631b

the post-combustion flue gas streams. The conventional amine-based solvents such as aqueous monoethanol amine (MEA) exhibit great CO_2 capture capacity; however, MEA's drawbacks include the corrosion of mechanical systems and vaporization and degradation losses of solvents during operation. Furthermore, the use of MEA solvent for CO_2 capture requires an energy intensive solvent regeneration process due to its high water content (70–85 wt%).[23–25]

Therefore, the development of alternative CO_2 capture media that address these issues is much coveted. A number of innovative organic and inorganic materials including solid adsorbents such as carbon nanotubes, zeolites, metal–organic frameworks (MOFs), amine-based solid materials, as well as liquid solvents such as ionic liquids and blended organic solvents are being developed.[26–34] They often exhibit high CO_2 uptakes even under low pressure conditions, simulating the flue gas environment, while their selectivities vary based on the existence of the task-specific functional groups.

Other desired characteristics of CO_2 capture media are a low energy requirement for the sorbent/solvent regeneration and long-term recyclability. As discussed for the case of the MEA solvent, the energy penalty associated with the desorption process is one of the most significant contributors to the operating cost.[35] In order to regenerate the CO_2 capture media, these materials are typically exposed to thermal, pressure, or vacuum swing processes.[36–39] In general, chemical sorbents with high selectivity towards CO_2 adopt thermal swings to regenerate the sorbents, and thus relatively robust thermal stability of the materials is required. Conversely, pressure swing regeneration processes can be employed for physical sorbents.[27]

Since most of the liquid CO_2 capture media are aqueous, a thermal swing regeneration process requires high pressure operation which further increases the overall capital cost as well as the potential environmental impacts throughout the system caused by the corrosive fumes. Therefore, liquid-like NOHMs, solvent-free nanoparticle-based organic hybrid systems, have been proposed as one of the promising candidates for CO_2 capture.[40] With NOHMs' negligible vapor pressure, there is no need for a high pressure regeneration unit during the thermal swing process and there are no issues with corrosive fumes.

For effective CO_2 capture, the organic–inorganic hybrid matrix of NOHMs could offer two distinct capture mechanisms *via* entropic and enthalpic effects. The chemical affinity, thermal stability, and rheological properties can be tuned to enhance these effects and optimize for CO_2 capture.[8,9,40] The entropic effect could be induced by structural arrangements of canopy species in NOHMs, while the enthalpic effect originates from relatively strong chemical interactions between CO_2 and task-specific functional groups, such as amines. Since the organic canopy species, which are tethered to the nanoparticles, act as a fluid medium, they can fill the gap between nanoparticles and prevent their agglomeration. Therefore, if the frustrated canopy species favor spontaneous ordering due to steric and/or entropic effects, each fluid unit of NOHMs consisting of the inorganic nanoparticles and grafted canopy could be arranged into a unique structural conformation. Furthermore, as small gaseous molecules (*i.e.* CO_2) are introduced into NOHMs and absorbed into the organic canopy layer, the free energy of the frustrated canopy could be reduced. The enthalpic effect is expected to account for most of the CO_2 capture; however, the structural change in the polymeric canopy can also influence the enthalpic effect *via* altering the accessibility and orientation of the CO_2-targeting functional sites. Therefore, it would be important to correlate the varied structures of the polymeric canopy to the CO_2 capture mechanisms. The ultimate goal of this area of research is to design NOHMs that optimize both entropic and enthalpic contributions to CO_2 capture.

As the first exploration into the solvating properties of NOHMs for CO_2 capture, this study focused on structural characterization and the underlying isolated entropic CO_2 capture mechanisms of the synthesized NOHMs without task-specific functional groups by observing specific intermolecular interactions.

Experimental

A series of NOHMs with ionically tethered amine terminated polymers (denoted as NOHM-I) were prepared. In order to synthesize NOHM-Is, LUDOX colloidal silica (7–22 nm in diameter, supplied by Sigma-Aldrich (Milwaukee, WI)) was diluted with deionized water to 3 wt% solution and added into 6 wt% solution of 3-(trihydroxysilyl)-1-propane sulfonic acid (supplied by Gelest Inc. (Morrisville, PA)). The acidity of the surface-modified SiO_2 nanoparticle suspension was adjusted to pH 5 by adding 1 M sodium hydroxide and the mixture was incubated at 343 K for 12 h with vigorous stirring. Next, the excess silane was removed *via* dialysis against deionized water (3.5k MWCO, manufactured by Pierce Biotechnology Inc. (Rockford, IL)) for 48 h. The dialyzed solution was then introduced into the cation exchange column (Dowex™ HCR-W2, manufactured by Dow Chemical Co.) to protonate the sulfonate group present on the surface of the nanoparticles. The resulting functionalized nanoparticle suspension was the common starting material for the preparation of NOHMs in the NOHM-I group. Once the polymer is selected for the synthesis of specific NOHMs, it was diluted to 10 wt% solution and added drop-wise to the functionalized nanoparticle suspension. In this study, the two polyetheramines ($H_3C(OCH_2CH_2)_m(OCH_2CH(CH_3))_nNH_2$) of different molecular weights, Jeffamine M-600 ($M_w \approx 600$) and Jeffamine M-2070 ($M_w \approx 2000$) provided by Huntsman Co. (The Woodlands, TX), were used as polymeric precursors for NOHMs. Once NOHMs were synthesized, the excess water was removed under reduced pressure at 308 K for 36 h. Finally, NOHM-Is with two different canopy species of Jeffamine M-600 (denoted as NOHM-I-PE600) and Jeffamine M-2070 (denoted as NOHM-I-PE2070) were obtained. The grafting densities of the polymeric canopy in two NOHMs were approximately 3.0 chains nm^{-2} which were measured by using a thermogravimetric analyzer (Q50, TA Instruments Inc. (New Castle, DE)). Scheme 1 illustrates the general structure of NOHMs in the NOHM-I group.

The prepared NOHMs samples were evaluated for their structures and interactions with CO_2 using a battery of analytical tools including a nuclear magnetic resonance

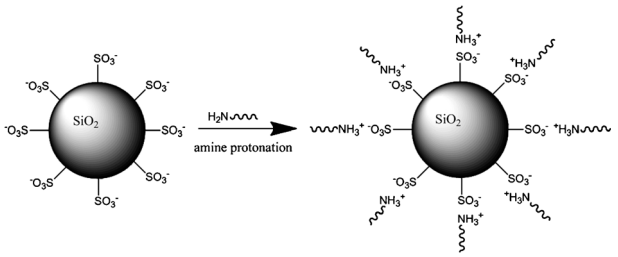

Scheme 1 Synthesis and schematic structure of NOHMs with ionically tethered amine terminated polymeric canopy species.

(NMR) and Fourier-transform infrared (FT-IR) spectrometers. For the NMR analysis, NOHMs samples were prepared by one of two methods, depending on the nature of the experiments. In the case of HSQC (Heteronuclear Single Quantum Coherence) and COSY (COrrelation SpectroscopY) analyses, a solution of 5 wt% Jeffamine M-600 and NOHM-I-PE600 in DMSO-d_6 were prepared in a standard 5 mm od NMR tubes. Neat samples for the ROESY (Rotating-frame Overhauser Effect SpectroscopY) experiments were prepared by using stem coaxial inserts (provided by Wilmad-Lab Glass (Vineland, NJ)). Jeffamine M-2070 and NOHM-I-PE2070 were carefully transferred to coaxial tubes (2 mm od) and the samples were vacuum dried at 313 K for one day to ensure the absence of any residual water in samples. In order to perform neat NMR measurements, the D_2O external referencing solvent is used with coaxial insert tubes. All the NMR experiments were performed using a Bruker DMX 500 MHz NMR spectrometer (Bruker BioSpin Co. (Billerica, MA)).

The FT-IR spectrometer (Nicolet 6700, Thermo Fisher Scientific Inc. (Madison, WI)) used in this study was equipped with a deuterated triglycine sulfate (DTGS) detector and an attenuated total reflectance (ATR) accessory (Golden Gate™ Supercritical Fluids analyzer, Specac Ltd. (UK)). The ATR optics with a PID temperature controller was topped with a high-pressure fluid cell, which has pressure range up to 42 MPa. The sample holding window of the ATR cell was a pyramidal diamond crystal (refractive index of 2.42, incident angle of 43° (±1°)) and the focusing lenses were made of ZnSe. With these specifications, the ATR cell offered single reflection measurements with a shallow sample penetration length of few microns. All spectra were measured with resolutions of 2 and/or 4 cm^{-1} in the 4000–525 cm^{-1} wavenumber region. All measured NOHMs samples reached equilibrium within 5 min, and the experiments were repeated at least twice under each temperature and pressure condition.

Results and discussion

In order to verify the structure of NOHMs, 2D NMR spectra were obtained. Fig. 1 shows 2D ^1H–^{13}C edited HSQC NMR spectra of NOHM-I-PE600 revealing that the peaks shift from the original locations of the peaks associated with pure Jeffamine M-600 (see ESI†). The edited HSQC experiments correlate the chemical shift of a proton with the chemical shift of a directly bonded carbon. Together with the ^1H–^1H COSY spectrum (see ESI†), the proton and carbon peaks were assigned as shown in Fig. 1. There were several interesting

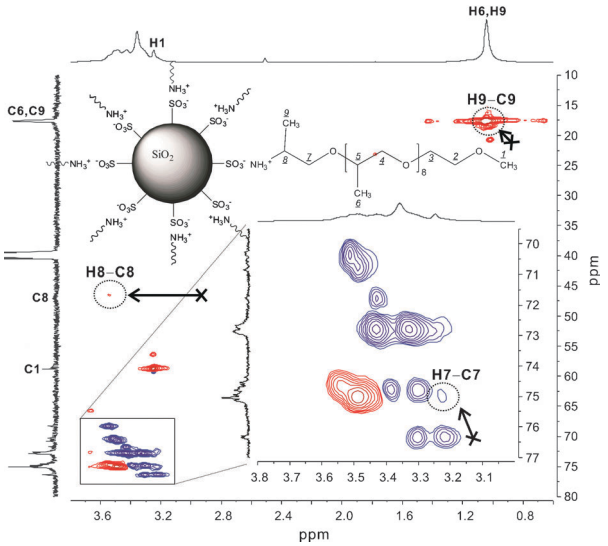

Fig. 1 2D ^1H–^{13}C edited HSQC NMR spectra of NOHM-I-PE600 in DMSO-d_6 at 298 K. Red contour exhibits carbons of CH or CH_3 (up) whereas blue exhibits CH_2 (down). Peaks in the range δ_H = 3.70–2.86 ppm of horizontal ^1H spectra are assigned to CH and CH_2 protons of canopy species. Cross marks indicate the original locations of the shifted peaks of Jeffamine M-600.

differences between the spectra of Jeffamine M-600 and NOHM-I-PE600. In Jeffamine M-600 spectra, two distinct doublets associated with two methyl groups, H6 (δ = 1.05 ppm, J = 6.3 Hz) and H9 (δ = 0.91 ppm, J = 6.4 Hz) were observed. However, in NOHM-I-PE600, the proton and carbon shifts of these methyls were found at δ_H = 1.05 ppm. This downfield shift of H9 suggests the formation of an ionic bond between the surface-modified SiO_2 core and the primary amines of polyetheramine. Since the oxygens in the sulfonate group deshielded the adjacent protons, a peak shift occurred. Compared to Jeffamine M-600, NOHM-I-PE600 spectra showed significantly different proton shifts downfield for both (H7, C7) methylene and (H8, C8) methine, which are adjacent to nitrogen. It is speculated that the proximity of the ionic bond has induced these large shifts. The ATR FT-IR spectrum verified this speculation by confirming the formation of an ionic bond, evidenced by the asymmetric (δ_a) and symmetric bends (δ_s) of $-NH_3^+$ of NOHM-I-PE600 at 1630 cm^{-1} and 1530 cm^{-1}, respectively (see ESI†).

The conformational behavior of the polymeric canopy of NOHMs was investigated *via* 2D ROESY NMR experiments (Fig. 2). The neat Jeffamine M-2070 sample is below or near the entanglement limit based on the literature values (M_e = 1600–2200 g mol^{-1} for PEO; M_e = 1287 g mol^{-1} for PPO).[10] Thus, in the neat Jeffamine M-2070, certain amounts of chain coiling may occur. On the other hand, in the case of NOHMs, it is speculated that the polymeric canopy and its associated counterion species are stretched out or ordered due to steric considerations—the tethered polymer chains must fill the space between nano-sized cores. When the polyether amine chains are coiled, ROEs may potentially be observed between protons on the opposite ends of the polymeric chains, such as between protons H1 and H8 or H9. Thus, the ROESY experiments should, in theory, be able to confirm this

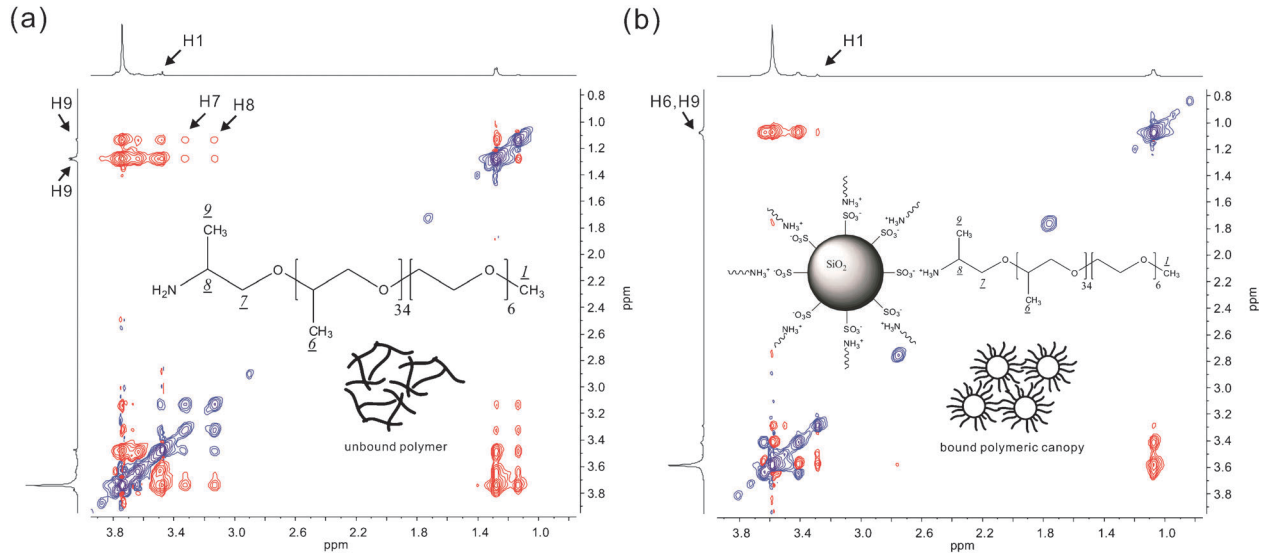

Fig. 2 Neat 2D ROESY NMR spectra of (a) Jeffamine M-2070 and (b) NOHM-I-PE2070 measured at 298 K. The blue contours exhibit diagonal and TOCSY (TOtal Correlation SpectroscopY, off diagonal), while the red contours exhibit ROEs. Peaks in the range δ_H = 3.8–3.5 ppm are assigned to CH and CH_2 protons of canopy species.

conformational behavior.[41] Moreover, if the hypothesis on the structural change during the synthesis of NOHMs is valid, such ROEs should be absent or be of smaller intensity.

As shown in Fig. 2(a), unbound polymers exhibit relatively strong ROE signals between H1 and H6/H9, which was expected since polymer chains exist in a randomly oriented state with possible chain coiling. On the other hand, in the case of the bound polymeric canopy species, the overall ROEs were decreased and the relative intensities between H1 and H6/H9 became significantly weaker (Fig. 2(b)). This implies that the organic canopy chains in NOHMs may be in a more ordered or stretched structural state compared to a freely oriented pure polymer.

Although the obtained ROEs data illustrated the possibility of the conformational structure of the ordered polymeric canopy of NOHMs, it is important to confirm these results using other experimental methods such as HSQC–ROE due to the severe proton overlap that is generally observed in the standard ROESY spectra. Furthermore, the conformational details of NOHMs packing may be important for understanding the mechanisms of CO_2 capture, and this study is on-going.

The packing of NOHMs fluid units was also visually observed using atomic force microscopy (AFM) and transmission electron microscopy (TEM) (see ESI†). As expected, NOHMs showed relatively ordered packing behavior with constant core-to-core distances. Both AFM and TEM images imply that NOHMs are self-suspended nanoparticle systems, and the polymeric fluid medium can fill the spaces between the nanoparticles.

In order to identify the CO_2 capture mechanisms of NOHMs, FT-IR spectra were obtained by employing the ATR technique. ATR FT-IR spectroscopy, which provides a small path length of an incident infrared beam, is one of the promising options to investigate the intermolecular interaction of specimens in highly absorbent media.[42] For the measurements, NOHMs samples were prepared as thin layers directly on the diamond crystal, and the sample cell assembly was pressurized with pure CO_2. As shown in Fig. 3(a), two distinct peaks of asymmetric stretching (ν_3 at 2335 cm^{-1}) and bending mode ($\nu_2 \approx 659$ cm^{-1}) of CO_2 absorbed in NOHMs were found. Aside from the CO_2 bands, the rest of the peaks showed trends of decreasing intensity with increasing CO_2 pressure. This trend was due to the volume increase of the NOHMs sample

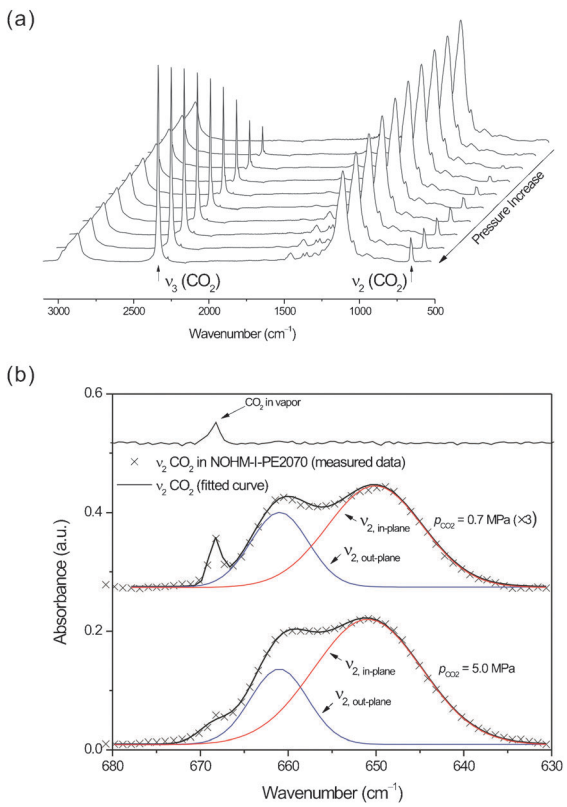

Fig. 3 (a) ATR FT-IR spectra of NOHM-I-PE2070 as a function of pressure (0 to 5.5 MPa at 298 K). (b) ATR FT-IR spectra of ν_2 bands of CO_2 in the vapor phase (top) and deconvoluted ν_2 bands of CO_2 absorbed in NOHM-I-PE2070 at 0.7 MPa (middle) and 5.0 MPa (bottom).

as it absorbed more CO_2.[43,44] For the C–O stretching bend, a noticeable peak shift to a higher frequency was observed while ν_3 showed a red shift (see ESI†). As the higher pressure of CO_2 was introduced into the sample cell, the peak of C–O stretching mode was continuously shifted to a higher wavenumber, indicating decreased interaction between the polymeric chains and their environment corresponding to the lowered liquid phase density.[42,45]

Fig. 3(b) further investigates the details of the ν_2 bending mode shown in Fig. 3(a). Compared to pure CO_2 in the vapor phase which shows a sharp single peak at 668 cm^{-1}, CO_2 absorbed in NOHM-I-PE2070 resulted in significantly differentpeak behaviors illustrating the occurrence of specific intermolecular interaction between CO_2 and NOHM-I-PE2070. It is known that functional groups including carbonyl group can act as an electron-donor for CO_2 *via* Lewis acid–base interaction.[46] Similarly, functional groups on NOHMs such as ether can be the Lewis base and interact with CO_2.[47] This Lewis acid–base interaction removed the double degeneracy of ν_2 bends, and, therefore, two peaks of 661 cm^{-1} (out-plane mode) and 650 cm^{-1} (in-plane mode) of CO_2 could be deconvoluted. This trend was continued at elevated pressures of CO_2.

It was also interesting that the area ratios of two deconvoluted ν_2 bending peaks associated with in-plane and out-plane modes were significantly changing as the CO_2 pressure increased from 0.7 to 5.5 MPa as shown in the bottom two spectra in Fig. 3(b). Thus, a series of ATR FT-IR experiments were performed to further investigate this phenomenon and all the obtained broad spectra were fitted by assuming peaks position of in-plane and out-plane modes of ν_2 at 650 cm^{-1} and 661 cm^{-1}, respectively.[46]

It is known that the ATR optics provoke less desired bands distortion of the relative intensities and introduce peak shifts to lower frequencies when compared to the spectrum obtained by a transmission method,[48] and thus it is rather difficult to estimate the absolute peak area ratio. However, the investigation of the relative peak area ratios in ν_2 bending modes of CO_2 absorbed in NOHMs and its pure canopy species could be useful to infer their structural differences or CO_2 packing patterns along the polymeric chains. As shown in Fig. 4, the change in the area ratios of two deconvoluted peaks during the CO_2 update in NOHM-I-PE2070 was quite different from that of the pure polymer (Jeffamine M-2070). This difference could mainly be caused by the changed intermolecular interactions between the polymeric chains based on the structural difference between freely oriented polymers and NOHMs. The packing patterns of absorbed CO_2 could vary if the entropy of the frustrated polymeric canopy of NOHMs is lower than that of free polymer systems. Another possibility could be the increased accessibility of the functional sites such as ether groups in NOHMs, which is also associated with the structural change. Recent *ab initio* calculation reported that the absorbance of the in-plane bending mode of CO_2 is about 3 times higher than that of the out-plane bending mode,[49] and the absorbance ratios of Jeffamine M-2070 shown in Fig. 4 approach that value, with some experimental variation possibly caused by the previously discussed band distortion of the ATR method. Recently, Yuan and Teja reported that for polymeric systems with electron donor–acceptor complexes the bending

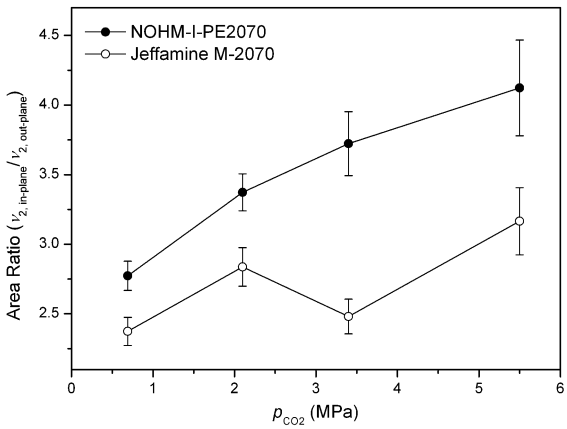

Fig. 4 Area ratio between deconvoluted ν_2 bending modes of in-plane and out-plane modes of CO_2 absorbed in NOHM-I-PE2070 and Jeffamine M-2070 as a function of CO_2 pressure at 298 K.

vibration frequencies could be observed in the order of; $\nu_{2,\text{in-plane}} < \nu_{2,\text{free}} < \nu_{2,\text{out-plane}}$, where $\nu_{2,\text{free}}$ represents 'free' CO_2 which is not significantly associated with Lewis basic sites such as ether.[50] Therefore, it may be possible to observe the additional $\nu_{2,\text{free}}$ peak between $\nu_{2,\text{in-plane}}$ and $\nu_{2,\text{out-plane}}$ bands in NOHMs. This could change the results of the absorbance ratios. These uncertainties associated with the peak assignments and the absorbance ratio estimation will be subjected to future investigations coupled with computational simulations.

Next, CO_2 capture capacity of NOHMs was calculated from the ATR FT-IR spectra using the Beer–Lambert law which expresses the relationship between the absorbance (A), the absorptivity (ε), the concentration (c), and the infrared path length (d). Unlike the transmission measurements, where the path length is kept identical to the thickness of the specimen, during the ATR FT-IR experiments the specimen is exposed to an evanescent electric field which undergoes exponential decay in its intensity at the interface between a crystal and the specimen. Therefore, the effective thickness of the evanescent wave (d_e) should be estimated from the reflective index.[51] The Beer–Lambert law is described as

$$A = \varepsilon c d_e \quad (1)$$

where d_e is the arithmetical mean between the effective path length for perpendicular ($d_{e\perp}$) and parallel ($d_{e\parallel}$) polarization. In order to calculate d_e, the refractive index of NOHM-I-PE2070 (n_D = 1.52) was measured by employing an ellipsometer (alpha-SE, J.A. Woollam Co., Inc. (Lincoln, NE)). The CO_2 capture capacities were quantified from the intensity of the ν_3 band,[42] and its molar absorptivity at high-pressure was assumed to be 1.0×10^6 cm^2 mol^{-1}.[52]

Fig. 5(a) shows CO_2 capture capacity of the tethered canopy (solvent) in NOHM-I-PE2070 as a function of pressure. Compared to the CO_2 capacities of pure Jeffamine M-2070, NOHM-I-PE2070 was slightly higher under the same CO_2 pressure conditions. Because the Lewis acid–base interaction between CO_2 and the ether group along the polymeric chains plays a major role in CO_2 capture mechanisms in this particular NOHMs system, it is speculated that the enhanced CO_2 capture capacity was structurally induced, as evidenced by; a more ordered or differently arranged structure of NOHMs

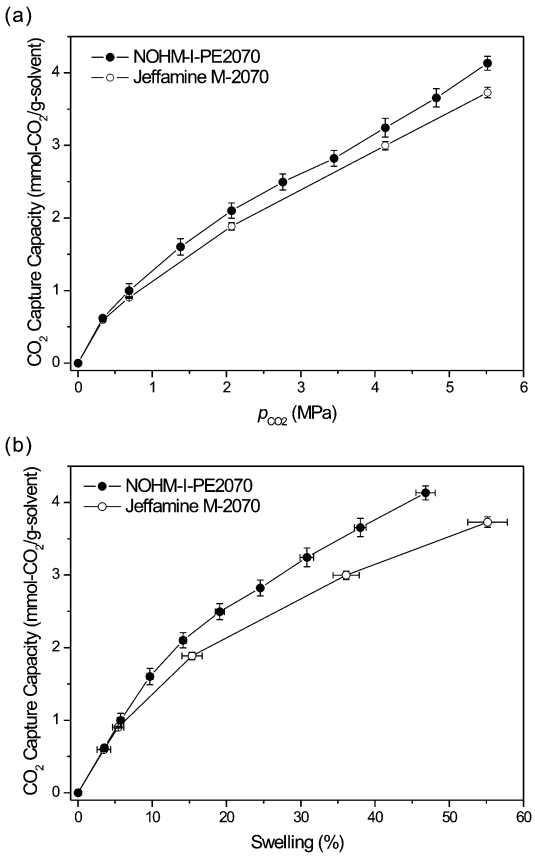

Fig. 5 CO_2 capture capacities of NOHM-I-PE2070 and Jeffamine M-2070 *vs.* (a) p_{CO_2} and (b) degree of swelling at 298 K.

versus a randomly oriented pure polymer. The structural change in NOHMs seems to offer a favorable pathway network for CO_2 to specific functional groups such as ether in canopy species.

It is important to note that although the enhanced CO_2 capture capacity of NOHM-I-PE2070 was relatively significant under high CO_2 pressure conditions, it is still far from the typical flue gas conditions (CO_2 partial pressure of $\sim$0.15 atm) found in coal-fired power plants. This is because the intended design of NOHMs samples used in this study was to isolate the entropic effect. The addition of task-specific functional groups and further structural consideration for canopy species such as grafting density, and designing of the canopy structure *via* manipulating interchain interaction, could maximize both enthalpic and entropic CO_2 capture, allowing for significantly improved CO_2 capture capacity that would be more favorable for industrial CO_2 capture conditions.

CO_2 absorption or impregnation processes result in swelling and change various mechanical and physical properties of polymers, such as reductions in viscosity and glass-transition temperatures.[53] Furthermore, less swelling of the solvent during CO_2 loading would allow a smaller reactor size which would be positive for the process economics. For NOHM-I-PE2070 and Jeffamine M-2070, the degree of swelling (S) was calculated by

$$S = \frac{A^0 d_e}{A d_e^0} - 1 \qquad (2)$$

where A^0, d_e^0, A, and d_e are the absorbance and the effective path length without and with CO_2, respectively. In order to calculate the degree of swelling, the absorbance of C–H stretching bands around 2865 cm^{-1} was selected by assuming that the absorptivity is not significantly affected by the concentration of CO_2 under different pressures. Thus, the change in the effective thickness was considered to be negligible. The volume change in NOHMs and polymer during CO_2 loading was calculated based on the integrated absorbances before and after exposure to CO_2 in the interval from 2700 cm^{-1} to 3000 cm^{-1}.

Since the CO_2 capture capacities of NOHM-I-PE2070 and Jeffamine M-2070 as a function of CO_2 pressure are different, their swelling (%) was plotted against CO_2 capture capacity rather than p_{CO_2} in order to compare their swelling behaviors. According to the results shown in Fig. 5(b), there is significantly less volume change in NOHM-I-PE2070 than in pure canopy species at the same CO_2 capture capacity. It can be explained that because the organic canopy matrix in NOHMs may exist as a more frustrated structure than pure polymeric canopy species by filling the gap between hard nanoparticles, as previously discussed, the packing of absorbed CO_2 could be different, allowing for increased CO_2 concentration between polymeric chains.

Finally, a multi-cycle CO_2 loading test was performed to evaluate the regenerative capacity of NOHM-I-PE2070. As shown in Fig. 6, the vacuum pressure swing regeneration process was achieved without any losses of efficiency and degradation of NOHM-I-PE2070 for the tested five capture–regeneration cycles. Since most CO_2 captured in this study were bound to NOHMs *via* relatively weak physical or Lewis acid-based interactions, the regeneration process did not require high temperature. However, amine-functionalized NOHMs which utilize stronger chemical interactions with CO_2 would require a combined pressure and temperature swing process for its regeneration.

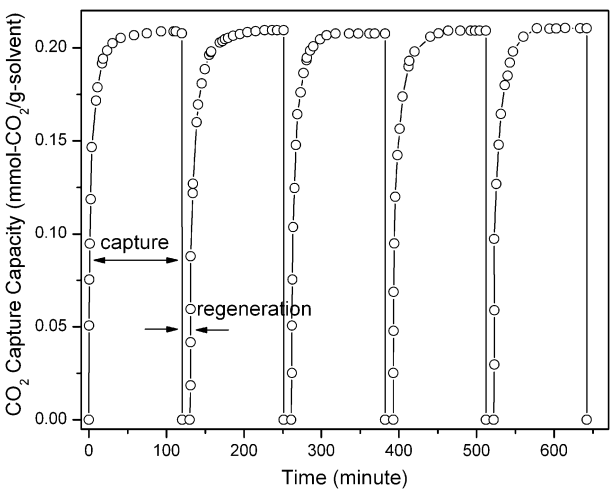

Fig. 6 Multi-cycle CO_2 loading test of NOHM-I-PE2070. CO_2 loading at 298 K under pressurized CO_2 (0.3 MPa) and solvent regeneration at 298 K under vacuum.

Conclusions

Newly synthesized NOHMs are a novel class of organic–inorganic hybrid materials that are highly tunable and have 'green' potential as alternative solvents for various energy and environmental technologies including CO_2 capture. In order to minimize the stronger enthalpic contribution during CO_2 capture, NOHMs were designed and synthesized in this study without task-specific functional groups, such as amines. The synthesized hybrid structure was characterized using a battery of analytical methods and the specific intermolecular interactions between CO_2 and NOHMs' polymeric canopy were identified through 2D NMR and ATR FT-IR spectroscopies. In particular, the relationship between the structural conformation of NOHMs and the underlying mechanisms for the CO_2 absorption behavior were investigated, focusing on the entropic contributions. Compared to unbound polymers, NOHMs exhibited enhanced CO_2 capture capacity, and different swelling behaviors of the canopy species suggest that the tethered organic species favor spontaneous ordering. This structural change could lead to effective CO_2 capture *via* the entropic effect.

Future studies include the investigation of other tunable parameters that would further optimize the entropic contribution such as canopy density and core-to-canopy size ratio. For the enthalpic contribution, various task-specific functional groups will be employed to increase CO_2 capture capacity of NOHMs. The study of the design of the canopy structure will also continue since, as evidenced in this study, it would play a critical role in the CO_2 capture performance of NOHMs. These results could also provide fundamental information needed for evaluating and developing other novel hybrid CO_2 capture materials.

Acknowledgements

This publication was based on work supported by Award No. KUS-C1-018-02, made by King Abdullah University of Science and Technology (KAUST). We are also grateful to Dr Luis Avila, Ms Dolly Shin and Dr Camille Petit for their help with the ATR FT-IR measurement.

Notes and references

1 T. V. Wenre and T. E. Patten, *J. Am. Chem. Soc.*, 1999, **121**, 7409.
2 S. Nuss, H. Bottcher, H. Wurm and M. L. Hallensleber, *Angew. Chem., Int. Ed.*, 2001, **40**, 4016.
3 A. Teteja, M. E. Macay, S. Narayanan, S. Ashokan and M. S. Wong, *Nano Lett.*, 2007, **7**, 1276.
4 M. E. Macay, A. Tuteja, P. M. Dexbury, C. J. Hawker, B. V. Horn, Z. Guan, G. Chen and R. S. Krishnan, *Science*, 2006, **311**, 1740.
5 P. Akcora, H. Liu, S. K. Kumar, J. Moll, Y. Li, B. C. Benicewicz, L. S. Schadler, D. Acehan, A. Z. Panagiotopoulos, V. Pryamitsyn, V. Ganesan, J. Ilavsky, P. Thiyagarajan, R. H. Colby and J. F. Douglas, *Nat. Mater.*, 2009, **8**, 354.
6 S. C. Warren, L. C. Messina, L. S. Slaughter, M. Kamperman, Q. Zhou, S. M. Gruner, F. J. DiSalvo and U. Wiesner, *Science*, 2008, **320**, 1748.
7 A. B. Bourlinos, S. R. Chowdhury, R. Herrera, D. D. Jiang, Q. Zhang, L. A. Archer and E. P. Giannelis, *Adv. Funct. Mater.*, 2005, **15**, 1285.
8 R. Rodriguez, R. Herrera, L. A. Archer and E. P. Giannelis, *Adv. Mater.*, 2008, **20**, 4353.
9 P. Agarwal, H. Qi and L. A. Archer, *Nano Lett.*, 2010, **10**, 111.
10 M. L. Jespersen, P. A. Mirau, E. Meerwall, R. A. Vaia, R. Rodriguez and E. P. Giannelis, *ACS Nano*, 2010, **7**, 3735.
11 A. B. Bourlinos, S. R. Chowdhury, D. D. Jiang, Y.-U. An, Q. Zhang, L. A. Archer and E. P. Giannelis, *Small*, 2005, **1**, 80.
12 A. B. Bourlinos, R. Herrera, N. Chalkias, D. D. Jiang, Q. Zhang, L. A. Archer and E. P. Giannelis, *Adv. Mater.*, 2005, **17**, 234.
13 A. B. Bourlinos, A. Stassinopoulos, D. Anglos, R. Herrera, S. H. Anastasiadis, D. Petridis and E. P. Giannelis, *Small*, 2006, **2**, 513.
14 A. B. Bourlinos, E. P. Giannelis, Q. Zhang, L. A. Archer and G. Floudas, *Eur. Phys. J. E*, 2006, **20**, 109.
15 S. C. Warren, M. J. Banholzer, L. S. Slaughter, E. P. Giannelis, F. J. DiSalvo and U. Wiesner, *J. Am. Chem. Soc.*, 2006, **128**, 12074.
16 A. A. Voevodin, R. A. Vaia, S. T. Patton, S. Diamanti, M. Pender, M. Yoonessi, J. Brubaker, J.-J. Hu, J. H. Sanders, B. S. Phillips and R. I. MacCuspie, *Small*, 2007, **3**, 1957.
17 S. T. Patton, A. A. Voevodin, R. A. Vaia, M. Pender, S. J. Diamanti and B. Phillips, *J. Microelectromech. Syst.*, 2008, **17**, 741.
18 Y. Zheng, J. Zhang, L. Lan, P. Yu, R. Rodriguez, R. Herrera, D. Wang and E. P. Giannelis, *ChemPhysChem*, 2010, **11**, 61.
19 A. B. Bourlinos, V. Georgakilas, N. Boukos, P. Dallas, C. Trapalis and E. P. Giannelis, *Carbon*, 2007, **45**, 1583.
20 A. B. Bourlinos, V. Georgakilas, V. Tzitzios, N. Boukos, R. Herrera and E. P. Giannelis, *Small*, 2006, **2**, 1188.
21 A. W. Perriman, H. Colfen, R. W. Hughes, C. L. Barrie and S. Mann, *Angew. Chem., Int. Ed.*, 2009, **48**, 6242.
22 J. L. Nugent, S. S. Moganty and L. A. Archer, *Adv. Mater.*, 2010, **22**, 3677.
23 G. T. Rochelle, *Science*, 2009, **325**, 1652.
24 H. Y. Huang, D. Chinn, C. L. Munson and R. T. Yang, *Ind. Eng. Chem. Res.*, 2003, **42**, 2427.
25 D. Aron and C. Tsouris, *Sep. Sci. Technol.*, 2005, **40**, 321.
26 D. M. Munoz, A. F. Portugal, A. E. Lozano, J. G. de la Campa and J. de Abajo, *Energy Environ. Sci.*, 2009, **2**, 883.
27 J. E. Rainbolt, P. K. Koech, C. R. Yonker, F. Zheng, D. Main, M. L. Weaver, J. C. Linehan and D. J. Heldebrant, *Energy Environ. Sci.*, 2011, **4**, 480.
28 F. Barzagli, F. Mani and M. Peruzzini, *Energy Environ. Sci.*, 2010, **3**, 772.
29 Q. A. Wang, J. Z. Luo, Z. Y. Zhong and A. Borgna, *Energy Environ. Sci.*, 2011, **4**, 42.
30 Y. Belmabkhout, R. Serna-Guerrero and A. Sayari, *Chem. Eng. Sci.*, 2009, **64**, 3721.
31 Y. Belmabkhout and A. Sayari, *Adsorption*, 2009, **15**, 318.
32 G. Qi, Y. Wang, L. Estevez, X. Duan, N. Anako, A.-H. A. Park, W. Li, C. W. Jones and E. P. Giannelis, *Energy Environ. Sci.*, 2011, **4**, 444.
33 A. Goeppert, S. Meth, G. K. Surya Prakash and G. A. Olah, *Energy Environ. Sci.*, 2010, **3**, 1949.
34 J. C. Hicks, J. H. Drese, D. J. Fauth, M. L. Gray, G. Qi and C. W. Jones, *J. Am. Chem. Soc.*, 2008, **130**, 2902.
35 N. MacDowell, N. Florin, A. Buchard, J. Hallett, A. Galindo, G. Jackson, C. S. Adjiman, C. K. Williams, N. Shah and P. Fennell, *Energy Environ. Sci.*, 2010, **3**, 1645.
36 E. S. Kikkinides, R. T. Yang and S. H. Cho, *Ind. Eng. Chem. Res.*, 1993, **32**, 2714.
37 S. Sircar, T. C. Golden and M. B. Rao, *Carbon*, 1996, **34**, 1.
38 B.-K. Na, H. Lee, K.-K. Koo and H. K. Song, *Ind. Eng. Chem. Res.*, 2002, **41**, 5498.
39 M. T. Ho, G. W. Allinson and D. E. Wiley, *Ind. Eng. Chem. Res.*, 2008, **47**, 4883.
40 K.-Y. A. Lin and A.-H. A. Park, *Environ. Sci. Technol.*, 2011, **45**, 6633.
41 D. Neuhaus and M. P. Williamson, *The Nuclear Overhauser Effect in Structural and Conformational Analysis*, Wiley-VCH, 2nd edn, 2000.
42 N. M. B. Flichy, S. G. Kazarian, C. J. Lawrence and B. J. J. Briscoe, *J. Phys. Chem. B*, 2002, **106**, 754.
43 M. G. Baschetti, E. Piccinini, T. A. Barbari and G. C. Sarti, *Macromolecules*, 2003, **36**, 9574.
44 I. Pasquali, J.-M. Andanson, S. G. Kazarian and R. J. Bettini, *J. Supercrit. Fluids*, 2008, **45**, 384.

45 J.-M. Andanson, F. Jutz and A. J. Baiker, *J. Phys. Chem. B*, 2009, **113**, 10249.
46 S. G. Kazarian, M. F. Vincent, F. V. Bright, C. L. Liotta and C. A. Eckert, *J. Am. Chem. Soc.*, 1996, **118**, 1729.
47 S. P. Nalawade, F. Picchioni, J. H. Marsman and L. P. B. M. Janssen, *J. Supercrit. Fluids*, 2006, **36**, 236.
48 M. Boulet-Audet, T. Buffeteau, S. Boudreault, N. Daugey and M. Pezolet, *J. Phys. Chem. B*, 2010, **114**, 8255.
49 Y. Park, *J. Supercrit. Fluids*, 2005, **36**, 154.
50 Y. Yuan and A. S. Teja, *J. Supercrit. Fluids*, 2011, **56**, 208.
51 N. J. Harrick, *Internal Reflection Spectroscopy*, Interscience Publishers, 1967.
52 P. G. Maiella, J. W. Schoppelerei and T. B. Brill, *Appl. Spectrosc.*, 1999, **53**, 351.
53 S. Uzer, U. Akman and O. Hortacsu, *J. Supercrit. Fluids*, 2006, **38**, 119.

